The modelled volume transports of CONTROL over the nested region are in close agreement with observational estimates. That applies to the East Australian Current, East Auckland Current and Tasman Leakage. Transports for Malvinas and Agulhas Currents are over and underestimated by roughly 10 Sv compared to observations, respectively. In SHIFT with exception of the East Auckland Current and Tasman Leakage, all transports show a decline in comparison to CONTROL. In INCREASE all transports with exception of the Tasman Leakage increases in comparison to CONTROL. The increasing transports in INCREASE are in agreement with the Sverdrup balance and more negative wind stress curl over the subtropical gyres. The weakening in SHIFT also aligns with changes in the large-scale wind stress curl pattern, which suggest an increase (see Figure S3). It is interesting to note that in SHIFT both the East Auckland Current and Tasman Leakage show an increase, while all previous studies found a seesaw behaviour (Behrens et al. 2019; Hill et al. 2008).

	Observations	CONTROL	SHIFT	INCREASE
East Australian Current (30°S) (southward)	22.1 Sv (Mata et al. 2000)	22.5 Sv	20.1 Sv	24.2 Sv
Malvinas Current (40°S) (northward)	41 Sv (Spadone and Provost 2009)	51.1 Sv	37 Sv	50 Sv
Agulhas Current (32°S) (southward)	73 Sv - 84 (Beal and Bryden 1999), (Beal and Elipot 2016)	58 Sv	53.8 Sv	67.8 Sv
East Auckland Current (eastward)	9 Sv (Stanton and Sutton 2003)	10.6 Sv	12.9 Sv	13.3 Sv
Tasman Leakage (westward)	10 Sv (Oliver and Holbrook 2014) 8-	11.3 Sv	16.3 Sv	8.5 Sv

Table T1. Mean volume transports for the CONTROL, SHIFT and INCREASE simulation. Values are averaged over the period 2015-2019 for East Australian Current, Malvinas Current, Agulhas Current, East Auckland Current and Tasman Leakage. Sv = 1×10^6 m3/s.

Figure S1a indicates that large interannual variability in Southern Ocean wind speed is present (zonal + meridional), without a meridional coherence between years. Figure S1b and S1c show how the zonal winds intensify over the period 2000-2019. North of ~42°S zonal winds are decreasing in strength (Figure S1c), while between 56°S to 60°S they intensify the largest by about 0.6% per year. Figure S1d shows that the maximum of the westerly winds shifts southward by 0.4° latitude per decade over the period 2000-2019.
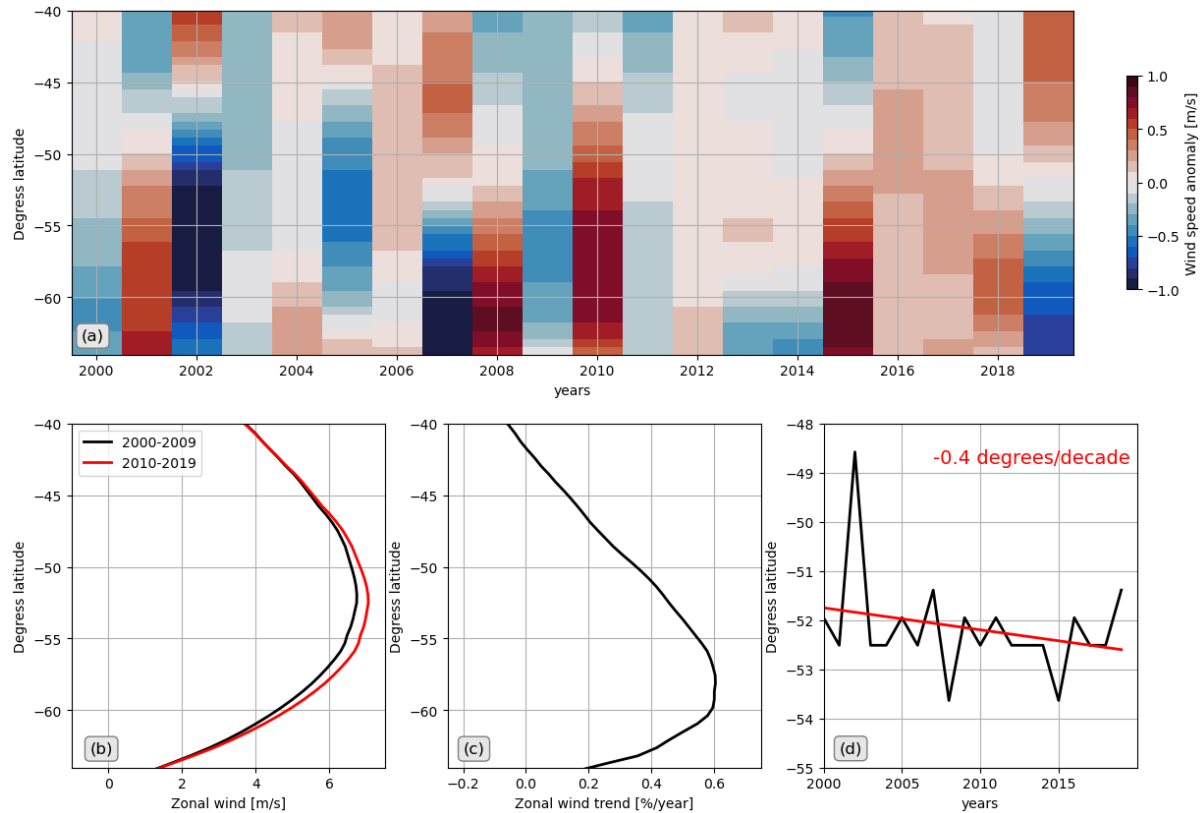

Figure S1. (a) Annual anomalies of zonally averaged (zonal + meridional) wind speeds in JRA55-DO relative to 2000-2019. (b) Zonal averaged zonal winds for the periods 2000-2009 (black) and 2010-2019 (red). (c) Percentage change per year between both periods in (b). (d) Location of maximum zonal winds (black) and linear trend (red). Red label provides the trend figure.

Figure S2a shows the northward Ekman transport over the Southern Ocean in CONTROL, which varies zonally and meridionally. Largest Ekman transports are found south of the STF. In SHIFT (Figure S2b) Ekman transports decrease, shown by the negative anomalies, over the STF. In INCREASE (Figure 2c) Ekman transports increase, shown by the positive anomalies, over the STF. Anomalies over the STF in INCREASE are largen than in SHIFT. (see also Figure 1)
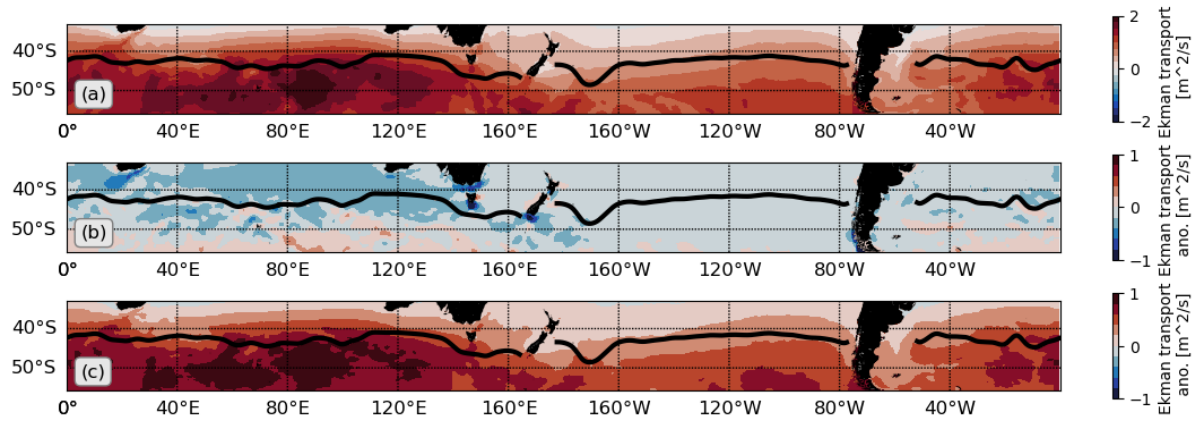

Figure S2. Ekman transport and anomalies averaged over the period 2015-2019. (a) CONTROL, (b) SHIFT-CONTROL, (c) INCREASE-CONTROL. The black line shows the mean location of the STF from CONTROL. Positive Ekman transports reflect a northward transport.

Figure S3a shows that heat fluxes over the western boundary currents (negative fluxes) and their extensions are directed from the ocean to the atmosphere in CONTROL. South of the STF heat fluxes are directed predominantly from the atmosphere into the ocean (positive fluxes). In SHIFT (Figure S3b) heat flux anomalies over the STF are mainly negative, which indicates a heat flux towards the atmosphere as this region warms. In INCREASE (Figure S3c) the response is more variable than in SHIFT over the STF. Over the boundary currents heat flux anomalies are negative as they intensify. Away from these currents heat fluxes are predominantly negative due to increased northward Ekman transports of cold water (Figure S2c). (see also Figure 1)
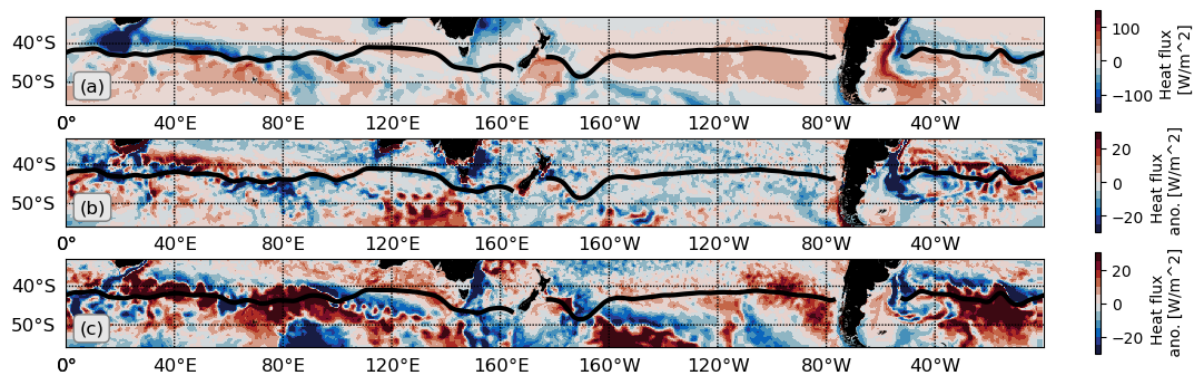

Figure S3. Surface heat flux and anomalies averaged over the period 2015-2019. (a) CONTROL, (b) SHIFT-CONTROL, (c) INCREASE-CONTROL. The black line shows the mean location of the STF from CONTROL. Positive surface heat fluxes indicate fluxes from the atmosphere into the ocean.

Figure S4a shows Ekman downwelling (negative values) over the subtropical regions and over the STF. In SHIFT (Figure S4b) Ekman pumping anomalies over the STF are mainly positive, which indicates less downwelling as the STF shifts south. In INCREASE (Figure S4c) Ekman pumping anomalies over the STF are mainly negative, which suggest more downwelling. (see also Figure 1)
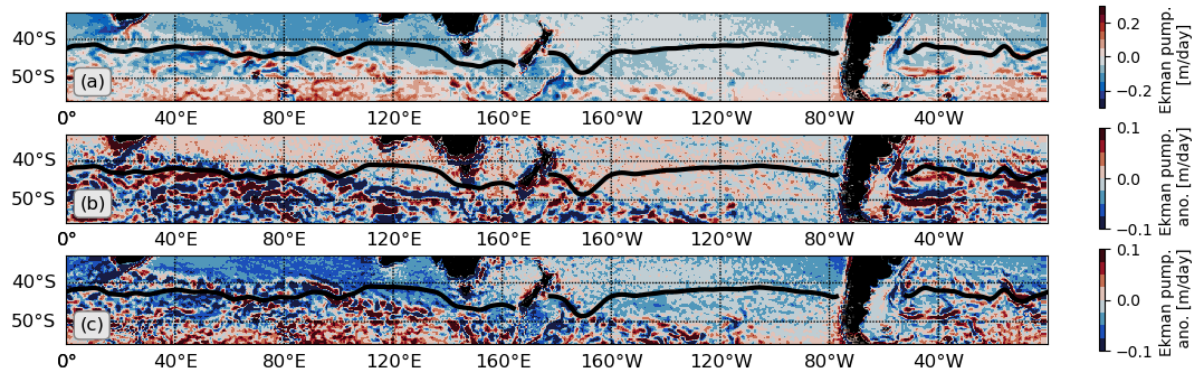

Figure S4. Ekman pumping and anomalies averaged over the period 2015-2019. (a) CONTROL, (b) SHIFT-CONTROL, (c) INCREASE-CONTROL. The black line shows the mean location of the STF from CONTROL. Negative Ekman pumping indicates a downward motion.

The temperature anomalies in SHIFT (Figure S5b) are positive over most parts of water column due to decreased Ekman transports. The location of the STF does not vary for this particular longitude. In INCREASE (Figure S5c) negative temperature anomalies are present over the upper water column due to increased Ekman transports. In INCREASE the STF shift northward over this longitude band.
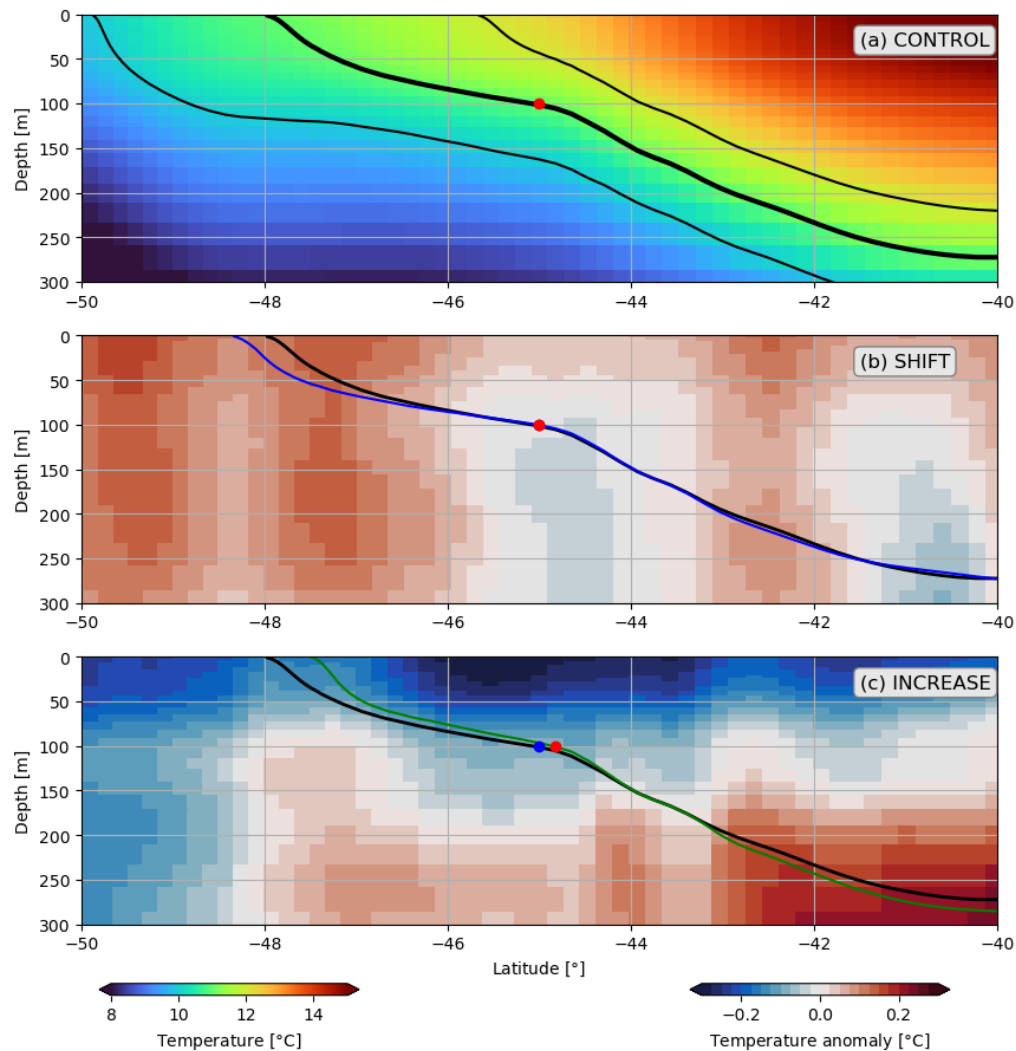

Figure S5. Temperature section and anomalies averaged between 180° to 160°W over the period 2015-2019. (a) CONTROL, (b) SHIFT-CONTROL and (c) INCREASE—CONTROL. Black contour lines in (a) mark the 10°C, 11°C (bold) and 12°C isotherm. The red dot marks the location of the STF (11°C isotherm at 100m depth). The blue and green lines in (b) and (c) mark the 11°C isotherm in SHIFT and INCREASE in relation to CONTROL (black line). The blue dots in (b,c) is the location of the STF from CONTROL, and the red dots represent the actual STF location in SHIFT and INCREASE, respectively.

Negative correlations over large parts of the STF in Figure S6a indicate that increased Ekman transports are associated with a decline in the top 100m temperatures. That is also reflected by the positive correlations in Figure S6b over the STF, which indicates that a northward shift of the STF, due a decline in temperatures causes additional heat fluxes from the atmosphere into the ocean.
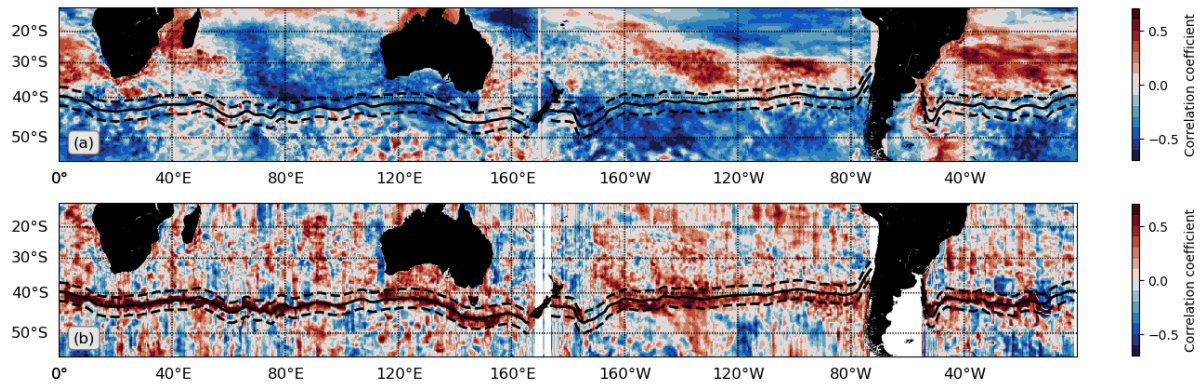

Figure S6. Pearson correlation coefficient between annual anomalies from NZ20 of (a) Ekman transport over the STF (±2.5° latitude) and top 100m averaged temperature, (b) meridional shifts of the STF and heat flux. The solid black line shows the mean location of STF from NZ20 for the period 2004-2019 and the dashed lines the ±2.5° latitude band over which the anomalies have been averaged for Figure 3b-c, 3e-f and 3h. Positive surface heat fluxes represent a heat flux from the atmosphere into the ocean.

The positive correlations south of the STF over large parts of the Southern Ocean in Figure S7a indicate that Chl-a concentration increase if top 100m temperatures increase in these regions, while they are negatively correlated north of the STF. This relation can then be linked to shifts in the STF (Figure S7b) where a southward shift of the STF is associated with a decline in Chl-a concentrations, south of the STF.
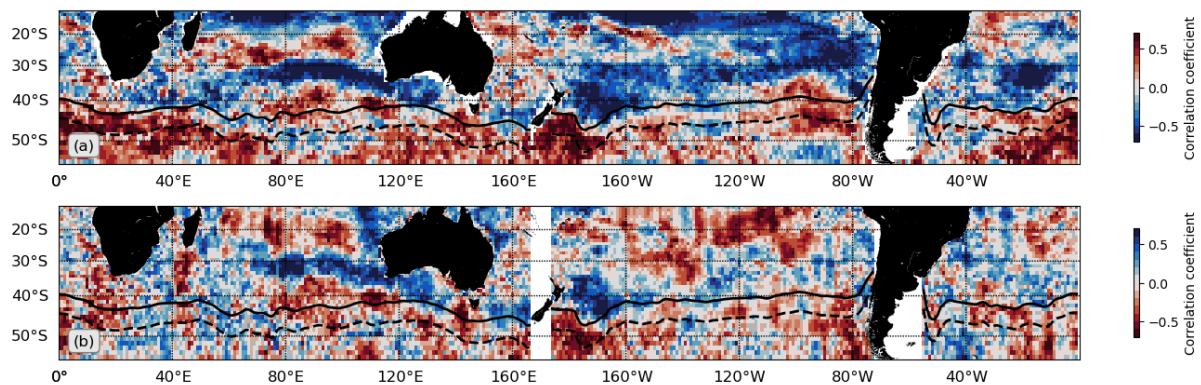

Figure S7. Pearson correlation coefficient between annual anomalies from Argo of (a) Chl-a and top 100m averaged temperature anomaly, (b) Chl-a and meridional shifts of the STF. The solid black line shows the mean location of STF from Argo for the period 2004-2019 and the dashed line the 5° southern boundary over which the anomalies have been averaged for Figure 3g and 3h. Note in (b) the colour scale has been inverted.

References:

Beal, L. M., and H. L. Bryden, 1999: The velocity and vorticity structure of the Agulhas Current at 32°S. *Journal of Geophysical Research: Oceans*, **104,** 5151-5176.

Beal, L. M., and S. Elipot, 2016: Broadening not strengthening of the Agulhas Current since the early 1990s. *Nature*, **540,** 570-573.

Behrens, E., D. Fernandez, and P. Sutton, 2019: Meridional oceanic heat transport influences marine heatwaves in the Tasman Sea on interannual to decadal timescales. *Frontiers in Marine Science*, **6,** 228.

Hill, K. L., S. R. Rintoul, R. Coleman, and K. R. Ridgway, 2008: Wind forced low frequency variability of the East Australia Current. *Geophysical Research Letters*, **35,** L08602.

Mata, M. M., M. Tomczak, S. Wijffels, and J. A. Church, 2000: East Australian Current volume transports at 30°S: Estimates from the World Ocean Circulation Experiment hydrographic sections PR11/P6 and the PCM3 current meter array. *Journal of Geophysical Research: Oceans*, **105,** 28509--28526.

Oliver, E. C. J., and N. J. Holbrook, 2014: Extending our understanding of South Pacific gyre spin-up : Modeling the East Australian Current in a future climate. *Journal of Geophysical Research: Oceans*, **119,** 2788--2805.

Spadone, A., and C. Provost, 2009: Variations in the Malvinas Current volume transport since October 1992. *Journal of Geophysical Research: Oceans*, **114**.

Stanton, B., and P. Sutton, 2003: Velocity measurements in the East Auckland Current north-east of North Cape, New Zealand. *New Zeal J Mar Fresh*, **37,** 195--204.